Available online at www.sciencedirect.com

ScienceDirect

Procedia CIRP 95 (2020) 103–108

www.elsevier.com/locate/procedia

20th CIRP CONFERENCE ON ELECTRO PHYSICAL AND CHEMICAL MACHINING

Mechanical and microstructural evolution of a 3D printed AlSi11Cu alloy

Jairo Alberto Muñoz Bolaños[a,] *, Denis Ten[a], Bazhenov Viacheslav[a], Alexander Komissarov[a], Alexander Gromov[a]

[a]*National University of Science and Technology "MISIS", Moscow 119049, Russia.*

* Corresponding author. Tel.: +79161624057 *E-mail address:* munos.bk@misis.ru

Abstract

Additive manufacturing (AM) processes have attracted a great interest in the scientific community during the last five years. This paper presents the 3D printing of a hypoeutectic Al alloy obtained by the Selective Laser Melting (SLM) technique. The initially printed material presented a cellular Al matrix microstructure with interconnected Si networks. Different tensile behaviors were found depending on the orientation of the specimens for both the initial material and after the annealing heat treatment. The specimens cut in the printing direction recorded lower ductility values, while those from the perpendicular plane and in the radial direction showed higher ductility and strength values.

Keywords: Al alloy; Microstructure; 3D printing; Mechannical properties;

1. Introduction

First impressions of Additive Manufacturing (AM) applicability date back 30 years in Austin Texas, where the first 3D printing machine was built [1]. However, research interest on AM processes has just increased in recent years. These processes base on joining metallic materials, either in the form of powder, wire, or sheets to shape 3D objects. In this way, metal components are built layer by layer, giving freedom of design and manufacturing flexibility[2–4]. These methods have the potential to revolutionize the elements design, due to factors like the speed at which parts are produced, the low number of manufacturing steps, low volumes of waste material, and also a large number of 3D printers entering the industry. For those reasons, sales of additive manufacturing systems have increased dramatically over the past five years [5]. Although additive manufacturing presents vast advantages, there are also specific problems related to the presence of pores, rough surface, lack of fusion between layers. However, perhaps the most important is anisotropy in the microstructure and mechanical properties, which today are considered the most striking topics for studies in the field of additive manufacturing. Many of these problems are related to the complex and cyclical thermal history the material is subjected as a result of the directional heat extraction, repetitive fusion between layers, and rapid solidification rates [6].

Nowadays there are different categories of additive manufacturing for metals like Selective Laser Melting (SLM) and Direct Energy Deposition (DED), whose are the most used and studied processes [1,7].

SLM is one of the best-known additive manufacturing processes. This process uses a high-energy laser beam to melt metal powders into a protected chamber with a controlled atmosphere that allows rapid solidification. Since this process does not require a mold, design, and production times are reduced in comparison with traditional processes [2].

Today, part of the success achieved by additive manufacturing is because the vast majority of metallic materials have been printed with great success through the different 3D printing techniques [8–10].

However, Al alloys, especially commercial ones such as the 2XXX, 5XXX, 6XXX, and 7XXX series, have been the most

10.1016/j.procir.2020.03.132

difficult materials in achieving their successful processing free of cracks and other defects. This behavior is associated with the high aluminum reflectivity, which makes it necessary to use high powers to melt it. On the other hand, the fact that the high cooling rates make the commercial alloys form micro-cracks because their alloying elements such as Cu, Mg, Zn, and Si promote wide solidification ranges resulting in the cracks appearance [11].

For this reason, Al-Si eutectic alloys have gained substantial importance due to their success and ease in printing by AM technologies as a result of their small range of solidification and weldability [12]. The big problem that this type of alloy presents is its low ductility (<4% true strain) and modest strength (<200 MPa yield stress) [6]. Several methods have been used to improve the ductility, such as scandium and expensive rare metals alloy. The adhesion of Zr particles helps to form nucleating phases of Al_3Zr promoting the formation of equiaxial structures with ultrafine grain sizes [12]. It has also been shown that the adhesion of Cu and Zn traces improves print quality and microstructural properties because Cu improves absorption capacity, and Zn does the same by promoting grain refinement [13,14].

Other strategies go through additional processes such as pre-heating of the powders before printing to improve their absorption capacity or involving procedures such as high-intensity ultrasound that helps to control the grain structure allowing to obtain ultrafine grain structures [15].

In this research work, we present the study of the mechanical and microstructural properties of a 3D printed AlSi11Cu alloy through tensile and compression tests in the reception state and after a stress relief heat treatment.

Nomenclature

$\delta\sigma/\delta\varepsilon$	Strain hardening rate
σ	True stress
ε	True strain
n	Hollomon strain hardening exponent
K	Material strength constant

2. Materials and methods

2.1. Selective laser melting process

The studied alloy was AlSi11Cu supplied in powder form with an average particle size of D_{10} 19.6 µm, D_{50} 40.4 µm and D_{90} 58.6 µm. Nominal composition described in Table 1. 20 mm diameter rods were printed on which the different mechanical and microstructural characterization specimens were extracted. The printing process was carried out by SLM, as shown in Fig 1a.

Table 1. Chemical composition of AlSi11Cu powder.

Element	Mg	Si	Ti	Mn	Fe	Cu	Al
Composition (wt %)	0.54	10.73	0.22	0.49	0.25	0.72	87.05

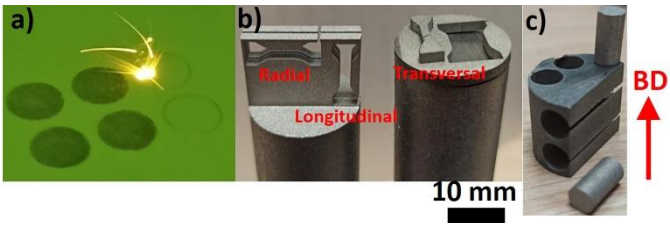

Fig 1. (a) SLM process; (b) tensile samples; (c) compression samples

Samples were manufactured using an SLM280HL printer equipped with a Yb laser with a 1064 nm wavelength. The system works with a laser power of 370 W, a scan speed of 1650 mm/s, and 130 µm hatch spacing. The whole process carried out in a controlled argon atmosphere.

2.2. Microstructure characterization

For microstructure characterization, optical microscopy (OM) using a Zeiss AX10 microscope was employed. The microstructure inside the fusion pools was characterized using a TESCAN VEGA SBH3 scanning electron microscope (SEM-EDS) with tungsten cathode from Oxford Instruments. The microstructure was revealed by a chemical treatment using Keller's reagent (2.5% HNO3, 1% HF, 1.5% HCl, and 95% distilled water).

2.3. Mechanical characterization

An annealing heat treatment was performed to remove the high residual stresses resulting from the SLM process by heating the material at 300 ° C for 2 hours and subsequent air cooling. Materials were subjected to uniaxial tensile and compression tests at room temperature with a constant strain rate of $1 \cdot 10^{-3}$ s^{-1}. The specimens were cut in different directions (parallel and perpendicular to the printing direction) using a wire electrical discharge machine, as indicated in Figs 1b-1c. Samples dimensions were 4 mm gauge length, 2 mm thickness, and 1.3 mm width for the tensile samples, and 5 mm diameter and 10 mm length for the compression ones.

3. Results and analysis

3.1. Microstructure evolution

To analyze the microstructure obtained by the SLM process, different planes of the printed samples were observed. Fig 2a shows the microstructure observed in the longitudinal plane (build direction vertical). At the same time, Fig 2b represents the microstructure seen from the transverse plane (build direction perpendicular to the plane). Initially, Fig 2a allows differentiating the cylinder-shaped fusion pools with their respective boundaries showing a typical cellular structure aligned in the building direction. Fig 2b indicates the different directions of the fusion pools according to the printing pattern of each layer showing an epitaxial growth with different pool

sizes. According to Garmendia et al. [13], it can be attributed to the partial re-fusion process of previously solidified layers.

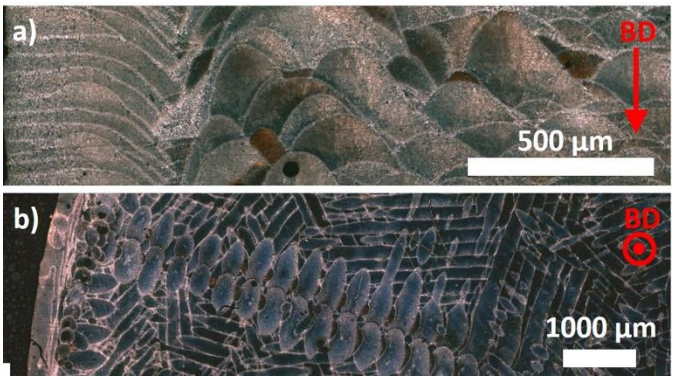

Fig 2. Microstructure evolution for the 3D printed alloy, (a) longitudinal plane (Build direction (BD) vertical); and (b) perpendicular to the building direction.

In addition to the OM characterization, Fig 3 shows the microstructure obtained employing SEM and Energy Dispersive X-Ray Spectroscopy (EDS). The formation of a coral-like structure forming eutectic Si networks on an Al cellular matrix is indicated.

Fig 3a indicates the existence of zones separated by a melt pool boundary (MPB) (highlighted by the yellow dashed line) in which different morphologies occur. Fig 3b, corresponding to the area marked with the red square b, shows a structure of elongated rich Si composition networks (brighter zones) and Al cells (darker zones) with a lower amount of Si according to the EDS spectrums. The approximate size of the Al cells in the square b is 2.5 µm, while on the other side of the MPB in the area highlighted by the square c, Fig 3c shows a more equiaxed cell pattern with approximate Al cell sizes of 1.5 µm.

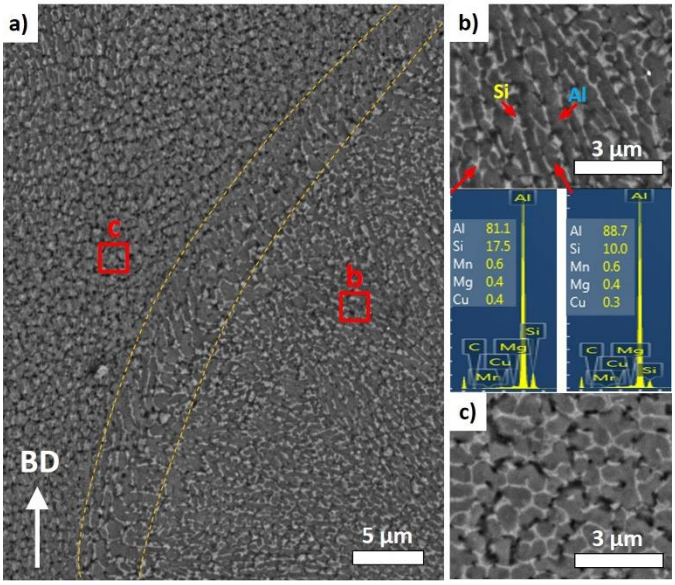

Fig 3. SEM images, (a) microstructure showing a melting boundary; (b) microstructure indicating the Al and Si phases corresponding with the b red square; (c) microstructure corresponding to the left side of the melting boundary (c square area).

These differences can be attributed to the proximity of zone c with areas of high thermal impact, e.g., triple points where different melting pools overlap. Similar behavior was reported by Griffiths et al. [12] in an Al-Mg-Zr alloy printed by SLM in which they reported smaller Al cells sizes at the base of the melt pools and larger cell structures in the center.

3.2. Mechanical properties

Fig 4 represents the tensile properties of the alloy, as well as the Considère criterion evolution for each of the tensile curves. The traction curves for the three directions shown in Fig 1b are indicated in Fig 4a for the as-printed material and after annealing treatment. After the annealing treatment, the material showed a strength reduction. However, this strength reduction was also reflected in the material ductility improvement. Table 2 summarizes the materials tensile properties. Higher values of maximum deformation for the annealing condition with values between 5.3% and 8.5% are observed. In contrast, the printing condition reached maximum deformations between 2.3% and 4.8%.

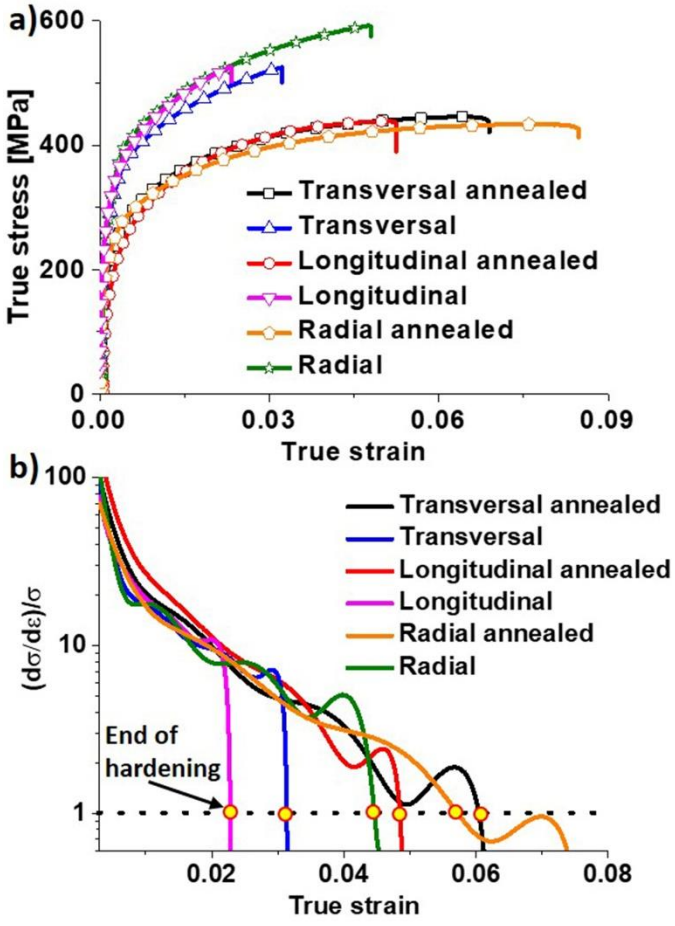

Fig 4. (a) True stress-strain curves; (b) Considère criteria evolution for all the conditions.

The tensile curves also allow observing the material anisotropy where the best strength and ductility properties correspond to the radial direction, followed by the transverse

direction and the worst performance for the longitudinal direction.

In order to observe the material ductility, the Considère criterion evolution is shown in Fig 4b, which establishes that the end of the homogeneous deformation in a material takes place when its strain hardening rate equals its strength, as indicated by equation (1) [16]:

$$\frac{\partial \sigma}{\partial \varepsilon} \leq \sigma \tag{1}$$

In this way, according to Fig 4b and Table 2, the as-printed material shows the smallest extensions of homogeneous deformation with values between 2.2% and 4.5%, with the longitudinal and radial directions displaying the smallest and highest ductility, respectively. Similarly, the annealed material also presented differences between the different directions, but with higher homogeneous deformation values, obtaining values between 4.8% and 6%.

Table 2. Mechanical properties for the alloy.

Condition	Yield stress (MPa)	Maximun stress (MPa)	Homogeneous deformation (%)	Total deformation (%)
Transversal	373.8	508.4	3.1	3.2
Longitudinal	378.9	514.3	2.2	2.3
Radial	393.1	565.12	4.5	4.8
Transversal annealed	264.7	419.8	6	6.9
Longitudinal annealed	289.5	425.7	4.8	5.3
Radial annealed	275.9	405.5	5.7	8.5

It worths mentioning that the strength and ductility values found in this study for both the as-printed and annealed condition stand out for their ductility with respect to other studies for similar alloys. For example, Garmendia et al. [13] reported a 461 MPa strength and 12% deformation for an AlSi10Mg alloy with a modified surface with Cu coating. Takata et al. [17] reported a strength of 476 MPa and deformations between 5.5 and 7.5 for AlSi10Mg obtained by SLM in the printing condition. At the same time, after annealing at 300 °C for 2 hours, they achieved a strength of 285MPa with deformation higher than 14%. On the other hand, Li et al. [18] studied the effect of solution heat treatment times in an Al-12Si eutectic alloy and found deformations higher than 25%, although the strength decreased from 350 MPa to less than 200 MPa.

To understand the anisotropy for the different directions of the tensile specimens, a study of the microstructure in the fracture zones of the materials was carried out.

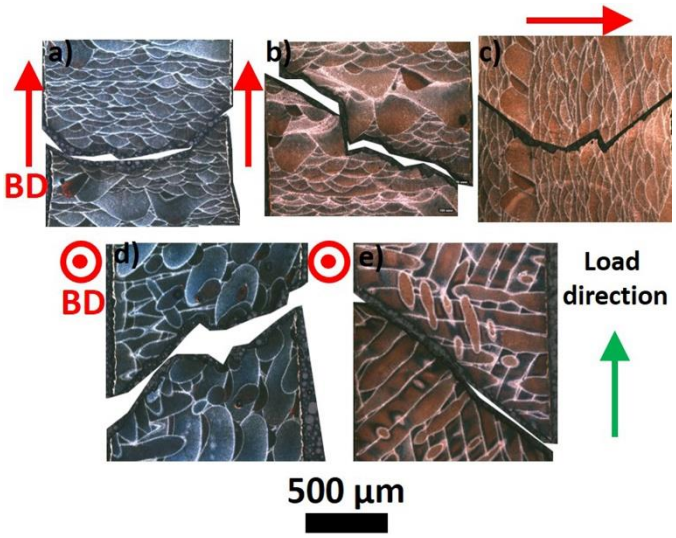

Fig 5. Tensile samples after fracture, (a) longitudinal; (b) longitudinal annealed; (c) radial annealed; (d) transversal; (e) transversal annealed.

From Fig. 5 it can be seen that depending on the orientation of the melt pools concerning the tensile load direction, there are different fracture paths. For example, Figs 5a and 5b show straight and smoothed fracture zones with indications of less plastic deformation in which the fracture is mainly performed as shedding of layers together with fracture by the melting boundaries of different layers. Meanwhile, Fig 5c shows a V-shape fracture zone where the material breaks through the fusion pools and by the pools boundary tracks. For the cross-sectional area Figs 5d-5e show that the fracture completely crosses the melt pools. These observations are in agreement with the research of Shifeng et al. [19], who studied the effect of the MPBs on the mechanical properties of stainless steel obtained by SLM. They also reported higher plastic deformation when the melt pools oriented perpendicular to the load direction.

Additionally, the vast majority of the fractures indicated in Fig. 5 follow a path oriented at ~45° to the load application except for the radial direction. This behavior is also reflected in the compression tests.

Fig 6a indicates the compression curves for the printed material and after annealing. With the compression curves, the previously observed in the tensile curves is corroborated. After annealing treatment, the material presented higher ductility and less strength. Similarly to the tensile test, the printed material breaks before the annealed one at a strain of ~ 26% following a path that forms 45° with the applied load.

Since the ductility of metallic materials, unlike their plasticity, depend on their hardening capacity, which in turn depends on the nature of the microstructure (i.e., grain size, dislocations), a simple strain hardening study is carried out for the two material conditions. Fig 6b shows the strain hardening exponent calculation through the equation proposed by Hollomon [20]:

$$\sigma = K\varepsilon^n \tag{2}$$

with σ and ε as the true stress and strain, K a material strength constant and n the strain hardening exponent. The

Hollomon equation fitting shows a good correspondence with the experimental data giving r^2 values of 0.98. Furthermore, the values of the constant K indicate a greater magnitude for the printed material than the annealed as a consequence of the strength differences.

Taking into account the Hollomon exponent evolution for both materials, Fig 6b demonstrates that after the annealing treatment, the material has the same value as in printing condition with strain hardening exponent (n) values of 0.23 and 0.24. Therefore, lower material ductility before and after annealing is due to an external fact of the microstructure, in this case, the possible existence of defects like pores, which are quite common defects in the SLM process. E.g. Tang et al. [21] reported the influence of porosity on the fatigue performance of an AlSi10Mg alloy obtained by SLM. They confirm the porosity formation by the oxidation of the vaporized metal, which made the material fail early.

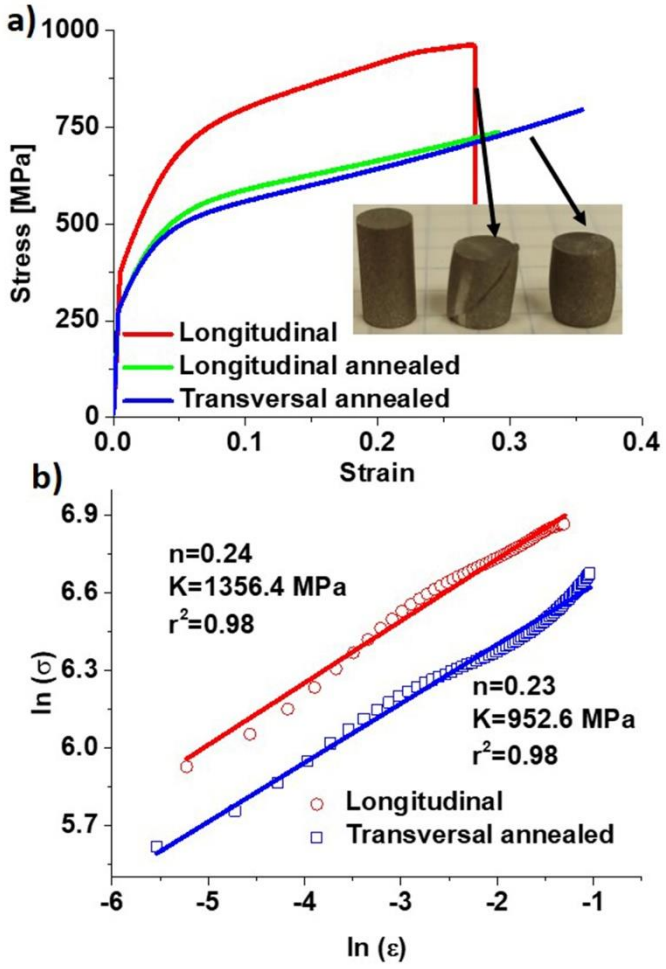

Fig 6. (a) compression curves before and after annealing treatment; (b) Hollomon strain hardening exponents before and after annealing treatment.

4. Conclusions

After obtaining an hypoeutectic Al alloy by AM using the SLM process, the next conclusions can be drawn:

A structure formed by melt pools oriented in the longitudinal direction in which the microstructure formed a cellular matrix of Al together with an interconnected coral type Si network.

The mechanical properties showed a clear anisotropy in the printed condition as well as in the annealed one, with higher strength and ductility in the radial direction, followed by the transverse direction and the longitudinal direction with the worst performance.

The material did not show changes in its strain hardening capacity after annealing by presenting similar Hollomon exponents, demonstrating that the lack of ductility in the alloy could be due to the existence of defects that caused its early fracture.

Acknowledgements

The authors gratefully acknowledge the financial support of the Ministry of Science and Higher Education of the Russian Federation in the framework of Increase Competitiveness Program of NUST «MISiS» (№ К4-2019-045), implemented by a governmental decree dated 16th of March 2013, N 211.

The authors also acknowledge the financial support of the Russian Science Foundation (RSF) (grant № 19-79-30025).

References

[1] W.J. Sames, F.A. List, S. Pannala, R.R. Dehoff, S.S. Babu, The metallurgy and processing science of metal additive manufacturing, Int. Mater. Rev. 61 (2016) 315–360. doi:10.1080/09506608.2015.1116649.

[2] J. Zhang, B. Song, Q. Wei, D. Bourell, Y. Shi, A review of selective laser melting of aluminum alloys: Processing, microstructure, property and developing trends, J. Mater. Sci. Technol. 35 (2019) 270–284. doi:https://doi.org/10.1016/j.jmst.2018.09.004.

[3] E.O. Olakanmi, R.F. Cochrane, K.W. Dalgarno, A review on selective laser sintering/melting (SLS/SLM) of aluminium alloy powders: Processing, microstructure, and properties, Prog. Mater. Sci. 74 (2015) 401–477. doi:https://doi.org/10.1016/j.pmatsci.2015.03.002.

[4] N.T. Aboulkhair, M. Simonelli, L. Parry, I. Ashcroft, C. Tuck, R. Hague, 3D printing of Aluminium alloys: Additive Manufacturing of Aluminium alloys using selective laser melting, Prog. Mater. Sci. 106 (2019) 100578. doi:https://doi.org/10.1016/j.pmatsci.2019.100578.

[5] J.C. Najmon, S. Raeisi, A. Tovar, 2 - Review of additive manufacturing technologies and applications in the aerospace industry, in: F. Froes, R. Boyer (Eds.), Addit. Manuf. Aerosp. Ind., Elsevier, 2019: pp. 7–31. doi:https://doi.org/10.1016/B978-0-12-814062-8.00002-9.

[6] K.G. Prashanth, S. Scudino, J. Eckert, Defining the tensile properties of Al-12Si parts produced by selective laser melting, Acta Mater. 126 (2017) 25–35. doi:https://doi.org/10.1016/j.actamat.2016.12.044.

[7] T.B. Sercombe, X. Li, Selective laser melting of aluminium and aluminium metal matrix composites: review, Mater. Technol. 31 (2016) 77–85. doi:10.1179/1753555715Y.0000000078.

[8] M. Tang, P.C. Pistorius, Anisotropic Mechanical Behavior of AlSi10Mg Parts Produced by Selective Laser Melting, JOM. 69 (2017) 516–522. doi:10.1007/s11837-016-2230-5.

[9] Y. Kok, X.P. Tan, P. Wang, M.L.S. Nai, N.H. Loh, E. Liu, S.B. Tor, Anisotropy and heterogeneity of microstructure and

mechanical properties in metal additive manufacturing: A critical review, Mater. Des. 139 (2018) 565–586. doi:https://doi.org/10.1016/j.matdes.2017.11.021.

[10] S.A.H. Motaman, F. Roters, C. Haase, Anisotropic polycrystal plasticity due to microstructural heterogeneity: A multi-scale experimental and numerical study on additively manufactured metallic materials, Acta Mater. 185 (2020) 340–369. doi:https://doi.org/10.1016/j.actamat.2019.12.003.

[11] T. Qi, H. Zhu, H. Zhang, J. Yin, L. Ke, X. Zeng, Selective laser melting of Al7050 powder: Melting mode transition and comparison of the characteristics between the keyhole and conduction mode, Mater. Des. 135 (2017) 257–266. doi:https://doi.org/10.1016/j.matdes.2017.09.014.

[12] S. Griffiths, J.R. Croteau, M.D. Rossell, R. Erni, A. De Luca, N.Q. Vo, D.C. Dunand, C. Leinenbach, Coarsening- and Creep Resistance of Precipitation-Strengthened Al-Mg-Zr Alloys Processed by Selective Laser Melting, Acta Mater. (2020). doi:https://doi.org/10.1016/j.actamat.2020.02.008.

[13] X. Garmendia, S. Chalker, M. Bilton, C.J. Sutcliffe, P.R. Chalker, Microstructure and mechanical properties of Cu-modified AlSi10Mg fabricated by Laser-Powder Bed Fusion, Materialia. 9 (2020) 100590. doi:https://doi.org/10.1016/j.mtla.2020.100590.

[14] K. Bartkowiak, S. Ullrich, T. Frick, M. Schmidt, New Developments of Laser Processing Aluminium Alloys via Additive Manufacturing Technique, Phys. Procedia. 12 (2011) 393–401. doi:https://doi.org/10.1016/j.phpro.2011.03.050.

[15] C.J. Todaro, M.A. Easton, D. Qiu, D. Zhang, M.J. Bermingham, E.W. Lui, M. Brandt, D.H. StJohn, M. Qian, Grain structure control during metal 3D printing by high-intensity ultrasound, Nat. Commun. 11 (2020) 1–9. doi:10.1038/s41467-019-13874-z.

[16] A. Considère, Memoire sur l'emploi du fer et de l'acier dans les constructions, Ann. Des Ponts Chaussées l Sem. 9 (1885) 574–775.

[17] N. Takata, H. Kodaira, K. Sekizawa, A. Suzuki, M. Kobashi, Change in microstructure of selectively laser melted AlSi10Mg alloy with heat treatments, Mater. Sci. Eng. A. 704 (2017) 218–228. doi:10.1016/j.msea.2017.08.029.

[18] X.P. Li, X.J. Wang, M. Saunders, A. Suvorova, L.C. Zhang, Y.J. Liu, M.H. Fang, Z.H. Huang, T.B. Sercombe, A selective laser melting and solution heat treatment refined Al-12Si alloy with a controllable ultrafine eutectic microstructure and 25% tensile ductility, Acta Mater. 95 (2015) 74–82. doi:10.1016/j.actamat.2015.05.017.

[19] W. Shifeng, L. Shuai, W. Qingsong, C. Yan, Z. Sheng, S. Yusheng, Effect of molten pool boundaries on the mechanical properties of selective laser melting parts, J. Mater. Process. Technol. 214 (2014) 2660–2667. doi:https://doi.org/10.1016/j.jmatprotec.2014.06.002.

[20] J.H. Hollomon, Tensile deformation, Aime Trans. 12 (1945) 1–22.

[21] M. Tang, P.C. Pistorius, Oxides, porosity and fatigue performance of AlSi10Mg parts produced by selective laser melting, Int. J. Fatigue. 94 (2017) 192–201. doi:10.1016/j.ijfatigue.2016.06.002.